Fe-Doped Zirconium Oxide Produced by Self-Sustained High-Temperature Synthesis: Evidence for an Fe−Zr Direct Bond

Paolo Ghigna,*,† Giorgio Spinolo,† Umberto Anselmi-Tamburini,† Filippo Maglia,† Monica Dapiaggi,† Gabriele Spina,‡ and Luciano Cianchi§

Contribution from the INCM, C.S.T.E./CNR, and Dipartimento di Chimica Fisica, Università di Pavia, Viale Taramelli 16, I 27100 Pavia, Italy, Dipartimento di Fisica, Università di Firenze, Via S. Marta 3, I 50139 Firenze, Italy, and IROE, Via Panciatichi 64, I 50127 Firenze, Italy

Received July 3, 1998

Abstract: The local structure of iron in Fe-doped cubic ZrO_2 produced by combustion synthesis was studied by Mössbauer spectroscopy and Fe-K edge extended x-ray absorption fine structure (EXAFS) and X-ray absorption near edge structure (XANES). Iron was found to be in its II oxidation state and to occupy two different sites of the fluorite ZrO_2 structure, both associated with some amount of disorder. One of the sites has been identified with the regular Zr position in 0,0,0, thus giving rise to substitutional Fe''_{Zr} (i.e., Fe atoms occupying the regular Zr position, with a net 2− charge, with respect to the lattice) defects, while the other site has been identified with the normally empty position at $^1/_2$, $^1/_2$, $^1/_2$, thus giving rise to interstitial $Fe_i^{\bullet\bullet}$ (i.e., Fe atoms occupying an interstitial position, with a net 2+ charge, with respect to the lattice) defects. For this last site, there is a short Fe−Zr distance (2.64 Å). This result, coupled to the quite small value of the Debye−Waller factor for this distance, gives evidence of a direct Zr−Fe metal-to-metal bond.

1. Introduction

The cubic form of zirconium oxide (zirconia) is well known for its mechanical, electrochemical, and optical applications.[1] Several preparative methods have been used for synthesizing, doping, and sintering this important material, as well as its composites with other ceramic or metallic phases. We have recently reported[2,3] that the self-sustained high-temperature synthesis (SHS) technique can be used to produce Me-YSZ (yttria-stabilized zirconia) cermets (Me = Ni, Co, Fe, Cu) and that these cermets show significant performance enhancements in their electrochemical applications with respect to those obtained with the traditional ceramic route based on the chemical reduction with hydrogen at high temperature of a previously sintered mixture of MeO and YSZ.[4]

SHS, or combustion synthesis, is a preparative technique based on the large heat effect of a heterogeneous chemical reaction. In this method, an external energy pulse is used to ignite the heterogeneous mixture of the reactant powders so that a (thermal and chemical) reaction wave is produced and propagates through the reactants in a stable self-sustaining manner.[5−10] YSZ-based materials can be produced by SHS either using oxidation with oxygen of Zr (metal) powders[11] or using the thermite reactions, which can be schematically described (for an MeO oxide) by

$$Zr + 2MeO \rightarrow ZrO_2 + 2Me$$

A well-appreciated property of SHS is its ability to produce solid materials in various metastable forms, which either were previously unknown or are accessible through other synthetic routes only with difficulty.[6,10] This ability has been related to the extremely high thermal gradients and reaction rates and temperatures of the SHS process, where the available reaction paths can be completely different from those active in conditions closer to thermodynamic equilibrium.

The fluorite-type structure of cubic zirconia is also well known for its excellent solvent properties for a fairly large variety of cations in different oxidation states. Aliovalent cations have been deeply investigated for their effect on defect chemistry and electrical properties of the phases. Lower valence cations replacing Zr (for instance, Ca^{2+}, Mg^{2+}, and Y^{3+}, just to quote the most known) are balanced by extrinsic ionized oxygen vacancies. Thus, doping dramatically increases the amount of oxygen vacancies and therefore increases the performance of the material as solid electrolyte by enhancing the diffusion coefficient of the oxide anion. Another field of interest concerns the ability of various dopants to extend the stability range of cubic zirconia (above 2650 K in the pure compound) down or close to room temperature.

From the point of view of crystal chemistry, there is a strong interest in the electronic structure and optical properties of the dopant as well as in various features of the local atomic structure

† Università di Pavia.
‡ Università di Firenze.
§ IROE.

(1) Stevens, R. *An introduction to zirconia*; Twickenham, England, Magnesium Elektron Ltd.: 1983; pp 1−22.
(2) Anselmi-Tamburini, U.; Arimondi, M.; Maglia, F.; Spinolo, G.; Munir, Z. A. *J. Am. Ceram. Soc.* **1998**, *81*, 1765−1772.
(3) Ghigna, P.; Spinolo, G.; Anselmi-Tamburini, U.; Maglia, F.; Morgante, N., to be published.
(4) Anselmi-Tamburini, U.; Chiodelli, G.; Arimondi, M.; Maglia, F.; Spinolo, G.; Munir, Z. A. *Solid State Ionics* **1998**, *110*, 35−43.
(5) Munir, Z. A.; Anselmi-Tamburini, U. *Mater. Sci. Rep.* **1989**, *3*, 277−365.
(6) Moore, J. J.; Feng, H. J. *Prog. Mater. Sci.* **1995**, *39*, 243−273.
(7) Moore, J. J.; Feng, H. J. *Prog. Mater. Sci.* **1995**, *39*, 275−316.
(8) Merzhanov, A. G.; Boroviskaya, I. P. *Dokl. Acad. Sci. USSR (Chem.)* **1972**, *204*, 429−432.
(9) Munir, Z. A. *Am. Ceram. Soc. Bull.* **1988**, *67*, 342−349.
(10) Varma, A.; Lebrat, J.-P. *Chem. Eng. Sci.* **1992**, *47*, 2179−2194.
(11) Anselmi-Tamburini, U.; Spinolo, G.; Munir, Z. A. *J. Mater. Synth. Proc.* **1993**, *1*, 323−333.

10.1021/ja982335a CCC: $18.00
Published on Web 12/31/1998

around the substitutional defect (distortions, association with vacancies, or several forms of clustering of point defects). For a recent systematic investigation with extended X-ray absorption fine structure (EXAFS) of the local structure of differently doped zirconia solid solutions prepared by the sol−gel route, the reader is referred to Li and co-workers.[12−14]

The dopant cations are always reported (or sometimes assumed) to enter the regular Zr sites as substitutional defects. This paper describes the different case of an iron-doped cubic zirconia solid solution that we have obtained during a systematic investigation of the feasibility of the SHS way to zirconia-based electrolytes and cermets. Peculiar features of this material are that iron enters two different sites and that one of these sites is the normally empty ($^1/_2,^1/_2,^1/_2$) position in the reference structure of cubic zirconia (the other one is the regular Zr site). To our knowledge, this is the first report on a cationic dopant that fills (at least partially) an interstitial position of cubic zirconia. The short distance between the regular Zr site and the interstitial site suggests the possibility of a direct Zr−Fe bond.

It must be finally noted that the solid solution discussed here has been produced only by performing SHS under the fastest available heating and cooling rates. Therefore, it is surely far from being a stable product and transforms into more conventional materials under fairly mild thermal treatments (i.e., at ∼750 °C).

2. Experimental Section

2.1. Synthesis. Samples of $Zr_xFe_{1-x}O_2$ have been prepared through a thermite reaction via combustion synthesis, starting from metallic Zr (Alfa Ventron >98%) and Fe_2O_3 (Aldrich 99%), according to the following general equation (neglecting the oxygen nonstoichiometry of $Zr_xFe_{1-x}O_2$):

$$(1 - x)Zr + [(2 - x)/3]Fe_2O_3 \rightarrow Zr_{1-x}Fe_xO_2 + [(4 - 5x)/3]Fe$$

Monoclinic ZrO_2 (Aldrich 99%) and metallic Fe (Aldrich 99.9%) were added as diluters in order to prevent an explosive behavior of the reaction. The composition of the starting mixture was Zr, 1.833 g; Fe_2O_3, 2.198 g; ZrO_2, 0.509 g; and Fe, 0.410 g; i.e., Zr and Fe_2O_3 are in a 3:4 molar ratio. The calculated adiabatic temperature was 2951 K; further details concerning the parameters of the thermite reactions via combustion synthesis are reported elsewhere.[2] All the materials were used without any chemical, grinding, or sieving treatment. The Zr powder, which is packed and mailed under water, was filtered and dried in air.

The starting powders were manually mixed in an agate mortar, isostatically pressed for 3 min at 200 MPa (2000 kg/cm^2) into pellets (diameter 10 mm, weight 3 g). The pellets were placed in a stainless steel SHS chamber and ignited with an electrically heated tungsten coil. The ignition coil was powered for 1−2 s until the formation of a stable thermal wave was detected. The reactions were performed under an atmosphere of 99.99% pure argon. Before each experiment, the reaction chamber was purged three times by pumping and back-filling. As soon as the reaction was completed, the pellet was dropped in water through an electrically controlled trap door placed under the reacting pellet.

The metallic fraction of the final product was eliminated by long treatments in hot HCl; the complete removal of the metal was checked by X-ray powder diffraction (XRPD).

2.2. Instruments and Methods. XRPD patterns were taken on a Philips 1710 instrument equipped with a copper anode operated at 40 kV and 35 mA, an adjustable divergence slit,[15] a vertical goniometer, and a graphite monochromator on the diffracted beam.

The Fe−K edge X-ray absorption spectra were collected at room temperature in transmission mode at the BM-29 beam line operating at the ESRF synchrotron radiation laboratory (experiment CH-372), using a double Si[311] crystal monochromator and ionization chambers filled with air as detectors. The monochromator is very stable in energy, so that no energy calibration is needed. For the measurements, the samples were mixed with polyethylene in a ball mill and then pressed into pellets. The edge jump for the Fe-doped ZrO_2 sample was about 0.3. To obtain a better signal-to-noise ratio, up to three scans were averaged for each sample. For X-ray absorption near edge structure (XANES) analysis, the spectra were normalized by subtracting the smooth preedge background fitted by a straight line and setting the absorption coefficient equal to 1 at an arbitrary point set at the energy at which there is an isobestic point in the FeO and Fe_2O_3 spectra (about 30 eV above the edge of FeO). An arbitrary energy scale was applied by setting the energy of the absorption maximum in the FeO spectrum equal to 0. The EXAFS was extracted by subtracting the smooth preedge background fitted with a straight line as for the XANES spectra and fitting the atomic postedge absorption with third-order polynomials. The EXAFS analysis was performed using the EXCURV97 code: amplitudes and phase shifts were calculated by the program. The correctness of the calculated phase shifts has been checked by fitting the FeO EXAFS. The fitted distances agree well with the crystallographic ones, the maximum shift being of 0.02 Å. The prepeak was isolated by fitting the edge jump with a sum of an erf function and an arctg function and then fitted with the required amounts of pseudo-Voigt function: this was done in order to take into account both the intrinsic Lorentzian broadening due to the finite lifetime of the core hole and the Gaussian broadening due to the finite energy resolution and bandwidth of the monochromator;[16] in the experimental conditions used here, the overall full width at half-maximum (fwhm) expected for a transition to a single level final state with zero energy width is 1.2−1.5 eV.

A polycrystalline powder sample was used to collect the Mössbauer absorption spectra. The sample consisted of very thin mixed particles of prepared substance and polyethylene pressed into a sample holder having a diameter of 20 mm, which was sealed with aluminized Mylar sheets. The reduced thickness of the sample was $t = 2$ mg of iron/cm^2. The [^{57}Co in Rh] source strength was about 25 mCi. A Gifford−Mac Mahon cryogenerator was used to cool the sample. The line broadening due to the cryogenerator vibrations was absolutely negligible (of the order of 10^{-2} G).

Electron microprobe analysis (EMPA) has been performed with a Link Microprobe Analyzer attachment of a Cambridge Stereoscan 200 microscope.

3. Results and Discussion

The effectiveness of the SHS in producing a metastable Fe-doped cubic ZrO_2 with fluorite structure (space group *Fm*3*m*) has been checked by inspection of the X-ray powder diffraction pattern, reported in Figure 1, of the material obtained at the end of the synthetic path described in the Experimental Section. Only very small amounts of impurities could be detected and are due to monoclinic ZrO_2, as shown by the inset in the same figure. To achieve the maximum sensitivity in the detection of impurities, the diffraction pattern of Figure 1 has been collected with a very long count time (15 s) and a step size of 0.02 °. This is reflected by the extraordinary peak intensity and by the detection of the β wavelength reflection of the (111) planes. According to the diffraction pattern, the cubic ZrO_2 sample appears as very well crystalline; in addition, the small fwhm of the diffraction peaks (about 0.15°) supports the conclusion of homogeneous chemical composition within the sample.

(12) Li, P.; Chen, I.-W.; Penner-Hahn, J. E. *J. Am. Ceram. Soc.* **1993**, *77*, 118−128.
(13) Li, P.; Chen, I.-W.; Penner-Hahn, J. E. *J. Am. Ceram. Soc.* **1993**, *77*, 1281−1288.
(14) Li, P.; Chen, I.-W.; Penner-Hahn, J. E. *J. Am. Ceram. Soc.* **1993**, *77*, 1289−1295.
(15) Anselmi-Tamburini, U.; Lupotto, P.; Spinolo, G. *Powder Diffr.* **1990**, *5*, 192.
(16) Ghigna, P.; Spinolo, G.; Scavini, M.; Anselmi-Tamburini, U.; Chadwick, A. V. *Physica C* **1995**, *253*, 147−155.

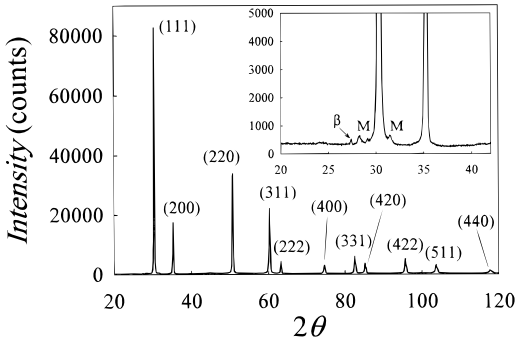

Figure 1. X-ray powder diffraction pattern of the Fe-doped ZrO_2. The Miller indexes refer to the cubic fluorite-type ZrO_2 structure. The inset shows the same pattern on an enlarged scale: the small peaks marked with M apparent between 27 and 32 ° are due to monoclinic ZrO_2. The peak marked with β is the β wavelength reflection due to the (111) planes (i.e., the most intense reflection).

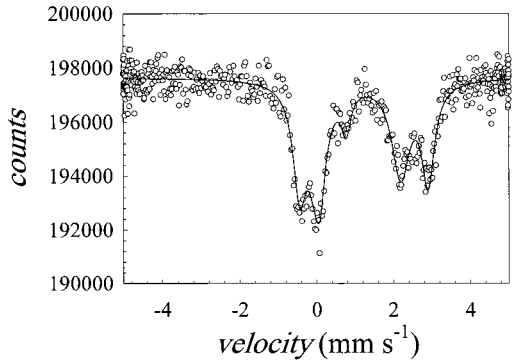

Figure 2. Mössbauer spectrum of the Fe-doped ZrO_2 at 14 K. Circles, experimental points; full line, fit according to the parameters reported in Table 1.

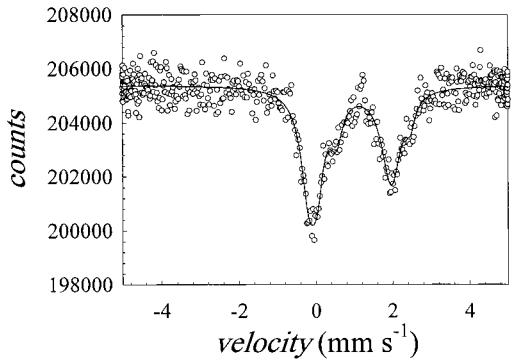

Figure 3. Mössbauer spectrum of the Fe-doped ZrO_2 at 300 K. Circles, experimental points; full line, fit according to the parameters reported in Table 1.

The amount of iron dissolved in the fluorite phase has been measured by EMPA and by a chemical method consisting of oxidizing and reducing treatments performed at 500 °C in pure oxygen and Ar/7% H_2 flow, respectively, and monitoring the weight change in a thermobalance: details will be reported elsewhere. Both methods agree with the $Zr_{0.9}Fe_{0.1}O_2$ formula.

Mössbauer spectra obtained at 14 and 300 K are shown in Figures 2 and 3, respectively. Spectra can be interpreted as consisting of at least three quadrupolar doublets. χ^2 values of 1069 and 1010, respectively, were obtained by fitting the 1024-channel spectra with three doublets (17 parameters): parameters are reported in Table 1. Line widths are much greater than the natural line width (0.2 mm/s). This means that the sites, especially site 2, are largely nonhomogeneous. On the basis of

Table 1. Mössbauer Spectra Fitting Parameters[a]

site	δ, mm s^{-1}	A/bl, 10^2 mm s^{-1}	ΔQ, mm s^{-1}	Γ, mm s^{-1}
		$T = 14$ K		
1	1.23 ± 0.01	2.33 ± 0.16	3.35 ± 0.02	0.40 ± 0.03
2	1.10 ± 0.01	3.18 ± 0.21	2.19 ± 0.03	0.57 ± 0.04
3	0.43 ± 0.02	0.72 ± 0.09	0.67 ± 0.04	0.30 ± 0.05
		$T = 300$ K		
1	1.26 ± 0.04	0.40 ± 0.18	2.41 ± 0.07	0.30 ± 0.12
2	0.95 ± 0.02	3.22 ± 0.26	2.04 ± 0.03	0.60 ± 0.05
3	0.16 ± 0.03	0.89 ± 0.11	0.76 ± 0.06	0.39 ± 0.07

[a] δ, chemical shift; A/bl, spectral weight; ΔQ, quadrupolar splitting; Γ, line width.

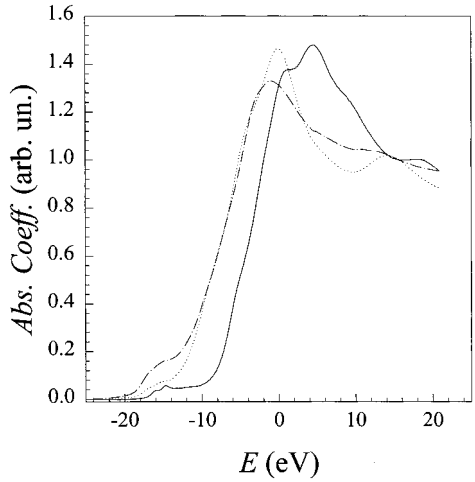

Figure 4. Fe−K edge XANES spectra of Fe_2O_3 (full line), FeO (dotted line), and Fe-doped ZrO_2 (dash−dotted line).

δ and ΔQ values, sites denoted by 1 and 2 can be attributed to Fe(II), and site 3 to Fe(III). The ratio between the absorption area related to site 3 and the absorption areas related to sites 1 and 2 is 0.13 at 14 K; taking into account that recoilless fractions may be different in different sites, one can estimate Fe(III) to be $\cong$10% of the total iron. The absorption area corresponding to site 1 collapsed on passing from 14 to 300 K. This fact can be explained by supposing that the potential at site 1 has a certain number of near minima. At low temperatures, the ion can perform oscillations inside one of these minima, while at high temperatures the ion has sufficient energy to pass from one minimum to another. The mean square displacement of the ion at low temperatures is therefore much less (and, consequently, the corresponding absorption area is much greater) than that at high temperatures. The decrease in the relative ΔQ can be explained in the same way: i.e., if the ion moves quickly from one minimum to another, the EFG components are averaged, so that ΔQ decreases.

The XANES spectra at the Fe−K edge are shown in Figure 4 for the present sample, FeO and Fe_2O_3, after preedge background subtraction and normalization as explained in the Experimental Section. The energy edge position is related to the oxidation state of Fe in the compound, according to the well-known "chemical shift". The feature at ca. −15 eV is usually called "prepeak", is due to the dipole-forbidden (but quadrupole-allowed) 1s $\rightarrow$ 3d transitions, and, as a consequence, is much more intense in the case of noncentrosymmetric environments, which allow Fe-3d O-2p mixing. It can be interpreted in terms of multielectronic configurations of 7 d electrons for Fe(II) [Co(II)] and of 6 d electrons for Fe(III) [Co(III)]:[17] this implies that one can obtain the spectroscopic terms for the $1s^1 3d^n$ final

(17) Calas, G.; Petiau, J. *Solid State Commun.* **1983**, *48*, 625−629.

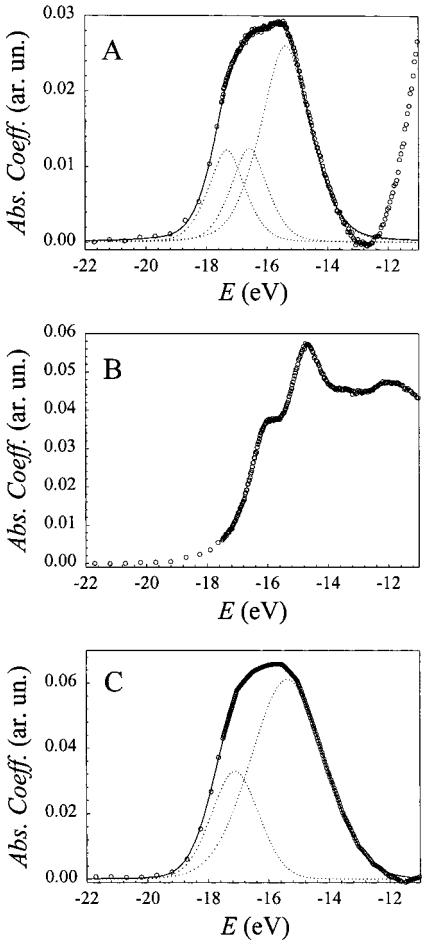

Figure 5. Fe−K edge prepeak in the XANES spectra of FeO (A), Fe_2O_3 (B) and Fe-doped ZrO_2 (C). Circles, experimental points; full line, total fit; dotted lines, partial fits with pseudo-Voigt functions.

state directly from the $3d^n$ multielectronic configuration, the only effect of the core hole being to change the spin multiplicity: transitions are then selected by the spin selection rule. Then, for Fe(II), the fundamental state with d^6 configuration is ^5D, and possible transitions are to final states ^5F and ^5P, with d^7 configuration. In the same way, for Fe(III) the fundamental state with d^5 is ^6S, and possible transitions are to the ^6D final state with d^6 configuration. Adding the crystal field splitting, one finds that the allowed transitions are for Fe(II) to final states $^5T_{1g}$, $^5T_{2g}$, and $^5T_{1g}$ and $^5T_1$, $^5T_2$, and $^5T_1$, in octahedral and tetrahedral field, respectively, and for Fe(III) to final states ^6E_g and $^6T_{2g}$ and $^6E_1$ and $^6T_2$ in octahedral and tetrahedral field, respectively. The prepeak of FeO is displayed in Figure 5a. FeO has a NaCl structure, with Fe in octahedral coordination. As a matter of fact, the formula is more correctly written as $Fe_{1-x}O$, and the defect structure is quite complicated, with Fe Frenkel defects (interstitial Fe in a tetrahedral interstice coupled to Fe vacancies). The prepeak can be fitted with three pseudo-Voigt functions: the two that are located at lower energy have fwhm of 1.7 eV and quite equal intensity, and the third peak at higher energy has fwhm of 2.3 eV, with a much larger intensity. This last peak is too wide for a single level. We think that this last peak is a superimposition of peaks due to regular Fe(II) in octahedral coordination and interstitial Fe in tetrahedral coordination: from the energy position this can be better assigned to Fe(III). By comparing the amplitudes, one can estimate the fraction of Fe(III) to be around 10%. For Fe_2O_3, the prepeak is shown in Figure 5b. The structure of Fe_2O_3 is a distortion of

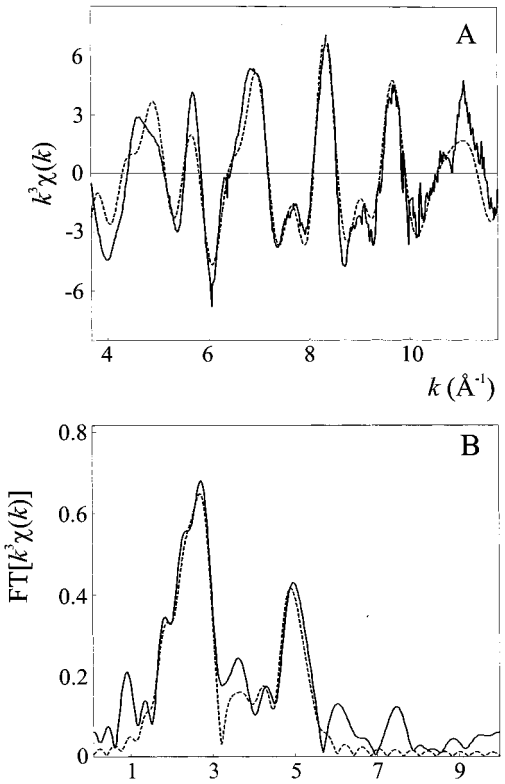

Figure 6. Fe−K edge EXAFS spectrum (A) and its Fourier transform (B) for the Fe-doped ZrO_2. Full line, experimental; dashed line, fitting according to the parameters shown in Table 2.

the Al_2O_3 type, with oxygen atoms forming a close-packed hexagonal arrangement, and Fe atoms in a noncentrosymmetric distorted octahedral coordination. In this case, the prepeak could not be resolved completely for the presence of an additional component at higher energy: this is of still unknown origin but has been already reported in the literature for other Fe(III) compounds.[17] In any case, two principal components, as expected for Fe(III) in an octahedral environment, are clearly apparent. The amplitude of the prepeak is compatible with the absence of the inversion center. For the Fe-doped ZrO_2 sample, (see Figures 5c and 4), the edge position is almost identical to that of FeO. Thus, the oxidation state of Fe in this sample is close to II, plus the eventual presence of Fe(III) in an amount of the order of 10%. The prepeak can be resolved in two components, of fwhm of 1.8 and 2.9 eV, both too large to be assigned to a single level. The amplitude of both is not compatible with the presence of an inversion center, and the structure of the prepeak is compatible with Fe(II) in a distorted cubic environment, plus a small amount (≅10%) of Fe(III) in a tetrahedral environment, as for FeO. The larger fwhm may indicate here the presence of more than one different site for Fe(II). Therefore, these results can be regarded as in good agreement with the Mössbauer results.

The EXAFS spectrum of the Fe-doped ZrO_2 sample is shown in Figure 6a and the corresponding Fourier transform in Figure 6b (full lines). The EXAFS Fourier transform can be regarded as a sort of pair correlation function: after correction for the phase shifts, it peaks near a coordination distance of a given coordination shell. The peak at ca. 1 Å in the EXAFS Fourier transform is due to some residual postedge background. The most emblematic feature of the EXAFS Fourier transform is the presence of an intense peak at ca. 2.5−2.7 Å. From the phase shifts and scattering amplitudes, this peak can only be attributed to Zr atoms. It should be noted that this is direct

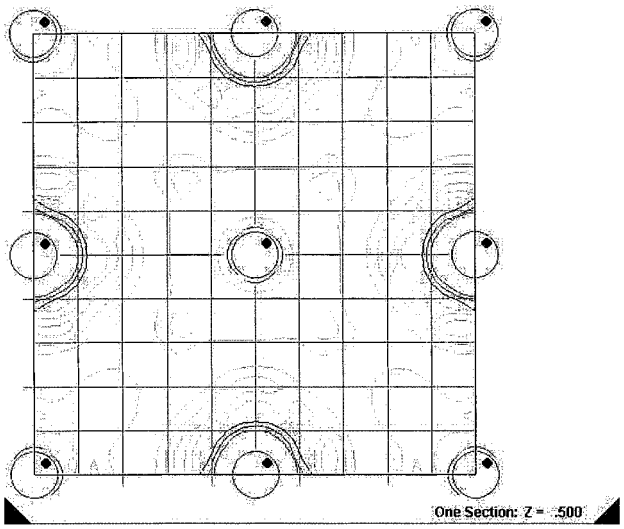

Figure 7. Fourier difference map as computed by the EXPO program starting from the XRPD pattern of Figure 1.

experimental evidence and does not rely on any fitting procedure of the spectrum. In the fluorite cubic ZrO_2 structure, a Zr coordination shell at 2.5−2.7 Å can be interpreted only by the presence of some Fe atoms in the (normally empty) interstitial position at $^1/_2$, $^1/_2$, $^1/_2$. To the authors' knowledge, this is the first time that direct evidence is given of interstitial doping atom presence in cubic ZrO_2.

This result can be confirmed by the analysis of the X-ray powder diffraction pattern. For doing this, the EXPO code[18] making use of direct methods was used. The structure has been resolved by imposing the presence of Zr and O atoms only. Then, in the Fourier difference map, a peak is clearly apparent in the $^1/_2$, $^1/_2$, $^1/_2$ position at the center of the cell (see Figure 7). Again, this is a direct experimental evidence and does not rely on any particular fitting procedure of the X-ray diffraction data.

As a matter of fact, Rietveld style analysis of the diffraction pattern was performed as well, giving further indication of the presence of some amounts of Fe at the cell center. In some details:

(1) A first refinement was done by supposing only the presence of substitutional Fe and refining the occupation fraction and the Debye−Waller factors: the result is the correct Zr:Fe ratio 9:1.

(2) A second refinement was done by supposing the presence of both substitutional and interstitial Fe and refining the occupation factors and the Debye−Waller factors of these two sites: the result is that 80% of Fe was found in the interstitial position.

(3) A last refinement was done by supposing equal amounts of substitutional and interstitial Fe and refining only the Debye−Waller factors of these two sites: the result is that the Debye−Waller factors assume a huge value.

This last result may be indicative of a large amount of static disorder. It should be noticed, however, that while EXAFS and Mössbauer spectroscopy are sensitive of the local structure, X-ray diffraction probes the long-range structure. The presence of different sites for the Fe doping atoms, each associated with an appreciable amount of disorder and distortion, makes the problem overwhelming for X-ray diffraction. For the above reasons, we must warn that the structural parameters as determined by Rietveld refinement are here of scarce physical significance. Therefore, we prefer to consider the last result as a simple confirmation of the presence of Fe in the $^1/_2$, $^1/_2$, $^1/_2$ position.

(18) Altomare, A.; Burla, M. C.; Camalli, M.; Carrozzini, B.; Cascarano, G. L.; Giacovazzo, C.; Guagliardi, A.; Moliterni, A. G. G.; Polidori, G.; Rizzi, R. *J. Appl. Cryst.* **1998**, *31*, 74−77.

Table 2. EXAFS Fitting Parameters for the Nonfiltered Spectrum of Figure 6[a]

shell	atom	*n*	*r* (Å)	*a* (Å^2)	r_0 (Å)
		Cluster 1: Substitutional Fe			
1	O	8	1.99(2)	0.039(4)	2.205
2	Zr	12	3.68(3)	0.035(7)	3.601
3	O	24	4.40(3)	0.013(4)	4.223
4	Zr	6	5.30(2)	0.015(4)	5.093
		Cluster 2: Interstitial Fe			
1	O	8	2.40(3)	0.05(1)	2.205
2	Zr	6	2.642(6)	0.0188(8)	2.547
3	O	24	4.26(3)	0.02(1)	4.223
4	Zr	8	4.75(2)	0.031(2)	4.411

[a] *n*, coordination number (not fitted); *r*, distance; *a*, Debye−Waller Factor; r_0, distance in the undistorted cubic ZrO_2.

To go further in the interpretation of the EXAFS, benefit can be taken from the indication of the Mössbauer and preedge analysis. Therefore, neglecting the presence of Fe(III), the whole EXAFS spectrum can be fitted by supposing the presence of almost equal amounts of Fe(II) in the regular substitutional 0,0,0 site and of Fe(II) in the interstitial site at $^1/_2$, $^1/_2$, $^1/_2$. The refinement of the occupation of each of these sites did not give a significant improvement of the quality of the fit, and in any case the fitted occupation did not deviate significantly from 0.5. Notably, this is the only way to get a reasonable fit of the spectrum with nonfiltered data.

The results of the calculation are displayed in Figure 6a and b as dotted lines; the corresponding parameters are shown in Table 2. The fit index, defined as

$$R_{\mathrm{EXAFS}} = \sum_i^N \frac{1}{\sigma_i} (|\chi_i^{\mathrm{ex}}(k) - \chi_i^{\mathrm{th}}(k)|) \times 100$$

where N is the number of data points, $\chi_i^{\mathrm{ex}}(k)$ and $\chi_i^{\mathrm{th}}(k)$ are the experimental and calculated EXAFS, respectively, is equal to 35.9%. For comparison, the corresponding distances in pure ZrO_2, calculated assuming a cell constant of 5.093 Å, as calculated from the XRPD pattern, are reported in the same table. The clusters used for the simulation are displayed in Figure 8. Multiple scattering paths have been taken into account in the calculation. This allows one to assign a given coordination shell to a given cluster; the symmetry group O_h (i.e., the point group pertinent to the 0,0,0 and $^1/_2$, $^1/_2$, $^1/_2$ sites in the *Fm*3*m* space group) was assumed for each of the two clusters, even if the Mössbauer and preedge analyses indicated some deviations from the pure cubic symmetry. This was done in order to keep the number of fitting parameters as low as possible.

The most important features are as follows:

(i) For the substitutional Fe atoms, the Fe_{Zr}−O distance is significantly smaller and for the interstitial Fe atoms the Fe_i−O distance is significantly greater than the corresponding Zr−O bond distance.

(ii) For the interstitial Fe atoms, the Debye−Waller factors for the Fe_i−Zr distance is quite small when compared to the corresponding parameter for the Fe_i−O bond length; this suggests the presence of a direct Fe_i−Zr bond. It should be noticed that the Fe_i−Zr distance is 2.64 Å, that is, of the right order of magnitude for a metal-to-metal bond length.

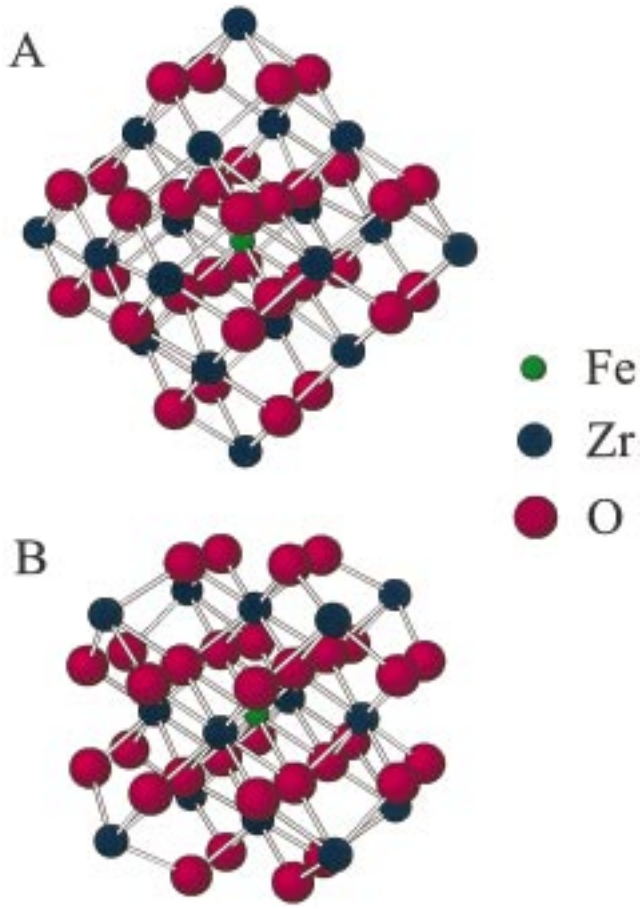

Figure 8. Clusters used in the EXAFS simulation. (A) Cluster for the Fe atom in the 0,0,0 position. (B) Cluster for the Fe atom in the $^1/_2$, $^1/_2$, $^1/_2$ position.

(iii) Generally, the Debye−Waller factors decrease as distance increases. As the EXAFS Debye−Waller factors reflect the correlation between the atomic displacements, and distant atoms are expected to have less correlated motion, this is contrary to what it is expected. This effect can be attributed to static distortions from the O_h symmetry around the doping atoms and/or to some amounts of static disorder; both these phenomena are expected to have a greater effect on the nearest coordination shells. Due to its time scale ($\cong 10^{-15}$ s), EXAFS is unable to distinguish static from thermal disorder: the presence of static disorder is suggested by the Mössbauer results. In addition, some deviation from the pure cubic environment for the Fe doping atoms is indicated by the preedge analyses. As a final comment, it could be recalled here that, according to the Mössbauer results, several minima are available for one of the Fe sites, the Fe atom being able to jump at room temperature among these minima. The identification of this site with the substitutional site or with the interstitial site is still an open problem, for which further experimental work (for examples, EXAFS and/or diffraction anomalous fine structure (DAFS) below room temperature) is required.

Some comments are due to the EXAFS data fitting procedure. As is apparent from Figure 6, all the major components of the EXAFS spectrum are adequately fitted. However, there are some additional components that are not fitted; the fitting of these components requires an addition of further coordination shells and, therefore, of further fitting parameters; therefore, it does not seem reasonable. As a matter of fact, one can apply a Fourier filtering procedure and then fit a filtered spectrum. Clearly, in this case one loses all the noise that appears as high-frequency components in the EXAFS Fourier transform, and therefore the main difficulty is that the statistical errors are without significance. However, for a better reference, we have done a fit of a filtered EXAFS spectrum (between 2.2 and 3 Å), as displayed in Figure 9, with only the Zr coordination shell. As the scattering amplitude of Zr peaks at greater k than that of O, we have truncated the EXAFS below $k = 5$ Å^{-1}: in this k range, the spectrum is dominated by the Zr shell, and the O shell at ≈2.4 Å, which is within the filtering window, is scarcely detectable. For this fit, the fitting parameters are displayed in Table 3, and $R_{EXAFS} = 16.2\%$. The distance and Debye−Waller factor obtained are in perfect agreement with those of Table 2.

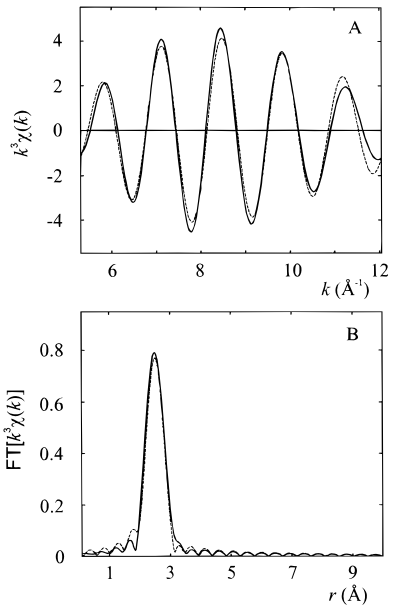

Figure 9. Fe−K edge EXAFS spectrum (A) and its Fourier transform (B) for the Fe-doped ZrO_2, filtered between 2.2 and 3 Å. Full line, experimental; dashed line, fitting according to the parameters shown in Table 3.

Table 3. EXAFS Fitting Parameters for the Filtered Spectrum of Figure 9[a]

shell	atom	n	r (Å)	a (Å^2)	r_0 (Å)
1	Zr	6	2.590(4)	0.0180(3)	2.547

[a] n, coordination number (not fitted); r, distance; a, Debye−Waller factor; r_0, distance in the undistorted cubic ZrO_2.

4. Conclusions

The main conclusions of this work are as follows:

(1) Combustion synthesis is an effective route for the preparation of Fe-doped cubic ZrO_2. The amount of Fe that can be dissolved, expressed as cation ratio, is 10%. Conflicting results (from a few % to more than 50% atom/atom) are reported in the literature about the solubility limit of iron in cubic zirconia materials prepared by sol−gel.[19−22] To the contrary, preliminary results by our group show that iron oxides (FeO or Fe_2O_3) do not react with pure monoclinic zirconia under usual isothermal−isobaric conditions.

(19) Beck, H. P.; Kaliba, C. *Mater. Res. Bull.* **1990**, *25*, 1161−1168.
(20) Davison, S.; Kershaw, R.; Dwight, K.; Wold, A. *J. Solid State Chem.* **1988**, *73*, 47−51.
(21) Inwang, I. B.; Chyad, F.; McColm, I. J. *J. Mater. Chem.* **1995**, *5*, 1209−1213.
(22) Ferrier, S.; Therasse, M.; Montel, G. *C. R. Acad. Sci. Paris* **1969**, *268*, C-1043−C-1046.

(2) Iron enters the ZrO_2 lattice mainly as Fe(II), allocated in roughly equal amounts in two different sites: each of these sites is quite disordered. The sites can be identified with the regular Zr site at 0,0,0 and the normally empty site at $^1/_2$, $^1/_2$, $^1/_2$. This gives rise, therefore, to roughly equal amounts of Fe''_{Zr} substitutional defects and $Fe_i^{\bullet\bullet}$ interstitial defects. The pertinent quasichemical equilibrium for Fe doping can therefore be written as $2FeO \rightleftarrows Fe''_{Zr} + Fe_i^{\bullet\bullet} + 2O_O^x$.

(3) For the interstitial $Fe_i^{\bullet\bullet}$, the shorter Fe−Zr distance is only 2.64 Å. This result, coupled to the quite low value for the Debye−Waller factor relative to this distance, suggests the presence of a direct Fe−Zr metal-to-metal bond. To the authors' knowledge, this is the first time that evidence is given for the presence of such a bond in an oxide.

Acknowledgment. This work has been partially supported by the Ministero dell'Università e della Ricerca Scientifica e Tecnologica of the Italian Government (MURST-40%). Dr. Adriano Filipponi is gratefully acknowledged for help during the XAS experiment and for helpful discussions of the results. Further thanks are due to Dr. Norman Binsted and Dr. Paul Stephenson for advice with the EXCURV97 program.

JA982335A